A LESS-TAPERED SIGNAL PROCESSING WINDOW
FOR POLARIMETRIC VARIABLES

Lindsey M. Richardson[a,*] and Igor R. Ivić[b,c]

[a] NEXRAD Radar Operations Center, Norman, Oklahoma, U.S. A.
[b] Cooperative Institute for Mesoscale Meteorological Studies, University of Oklahoma, Norman, Oklahoma, U.S.A.
[c] NOAA/OAR/National Severe Storms Laboratory, Norman, Oklahoma, U.S.A.

1. INTRODUCTION

Signal processing windows can be used to reduce spectral leakage when transforming signals from the time domain to the frequency domain for analysis and processing. Weather radars, such as the Weather Surveillance Radar – 1988 Dual-Polarimetric-Doppler (WSR-88D), can use the windowed data for clutter filtering or moment/variable estimation. Algorithms such as GMAP (Siggia and Passarelli 2004), CLEAN-AP (Torres and Warde 2014; Warde and Torres 2017), and SZ-2 (Saxion et al. 2007) all use frequency domain information.

Windows may also be used to facilitate achieving effective beamwidth requirements related to a rotating antenna transmitting with a pencil beam. For example, the WSR-88D System Specifications (WSR-88D ROC 2018a) states that scanning strategies must be performed in a certain number of seconds with no fewer than 15 pulses. This limits rotation rates to specific ranges; very fast speeds do not receive the required minimum number of pulses while slower speeds with more pulses do not meet timing requirements. Rotating the antenna requires consideration of the effective beamwidth to achieve desired azimuthal resolution for phenomenon detection. Signal processing windows applied to the beam pattern can mitigate some effects from rotating the beam, though it can never be improved beyond the natural beamwidth produced by the antenna.

The WSR-88D uses different scanning strategies based on the meteorological returns of interest and includes using higher azimuthal resolution at lower elevation angles. A von Hann window was selected for Base Data moments of Reflectivity (Z), Velocity (V), and Spectrum Width (W) at the lower elevation angle to achieve an effective beamwidth close to the natural beamwidth of 0.96° which can be split in half for enhanced detection of specific small-scale features (Brown et al. 2002; Warde et al. 2005; Torres and Curtis 2006, 2007; WSR-88D ROC 2008).

Windows with strong sidelobe suppression, i.e. those with a first sidelobe reaching a lower magnitude such as the Blackman and Blackman-Nuttall, can be used by clutter identification and/or mitigation algorithms to isolate or remove clutter from the spectra. In regions without clutter, windows with higher sidelobes such as the Hamming, von Hann, and Rectangular are used.

Signal processing window characteristics impact

estimation bias and variance which may be notable depending on the estimator. Work by Melnikov and Zrnić (2004, 2007) show that the Dual-Polarization variables of Differential Reflectivity (ZDR), Correlation Coefficient (RHO), and Differential Phase (PHI) are more sensitive to noise compared to Base Moments. This can appear as visual variability in data fields and has the potential to impact derived products created by downstream algorithms. When Dual-Polarization (DP) capability was added to the WSR-88D network using Simultaneous Transmit and Receive mode, the von Hann window remained the default window selection at lower elevation angles in regions without clutter (WSR-88D ROC 2010; WSR-88D ROC 2013). Selection of the von Hann window came from availability of existing processing methods and time constraints encountered during development and deployment. A study of which window should be used for Dual-Polarization variables in regions without clutter had yet to be performed.

Several signal processing windows with varying degrees of tapering are explored herein to determine how the window selection impacts DP variables in regions without clutter. Window impacts in relation to clutter filtering and clutter filtering algorithms are beyond the scope of this study. Quantitative metrics are investigated for identifying impacts on bias, variance, and effective beamwidth on non-derived (or raw) data products. Qualitative impacts are considered for visual interpretation and potential differences in derived products from algorithms.

2. WINDOW CHARACTERISTICS

WSR-88D systems operationally use the von Hann, Hamming, and Rectangular windows for regions without clutter. These windows come from the Generalized Cosine family of windows described as:

$$w(n) = \alpha + (\beta)cos(2\pi(n + 0.5)/M) \qquad (1)$$

where M is the number of samples and $n = 0, \ldots, M\text{-}1$. Coefficients α and β are generally values resulting in the sum of α and β equal to 1.0 for normalization (Harris 1978). The coefficients are directly related to the amount of tapering and amplitude at the endpoints of the window. Clutter filtering schemes generally require endpoints of 0.0 amplitude to prevent spectral leakage, but that requirement is not a priority in the non-clutter regions of focus in this study. Window endpoints are allowed to range from 0.0 to 1.0 which match the existing von Hann and Rectangular windows respectively.

The window shape in the time domain and its associated tapering directly impact azimuthal effective

Corresponding author address: Lindsey M. Richardson, Radar Operations Center, Norman, OK, e-mail: Lindsey.M.Richardson@noaa.gov
AMS 39th ICRM

beamwidth. For a reflector antenna scanning at a constant elevation angle, the azimuthal effective antenna beam pattern corresponding to processing M samples with a data window, w, is given by (Zrnić and Doviak 1976; Doviak and Zrnić 2006, section 7.8):

$$f_{eff}^4(\varphi) = \gamma \sum_{m=0}^{M-1} f^4(\varphi - M\Delta\varphi) w^2(n) \qquad (2)$$

where $f^4(\varphi)$ is the intrinsic two-way antenna beam pattern, γ is a normalization factor such that $f_{eff}^4(0) = 1$, φ is the azimuthal angle relative to the beam center and $\Delta\varphi$ is the azimuthal angle that describes the antenna movement in the time between transmitted pulses. Window shapes and tapering will be described for the time domain and the Fast Fourier Transform result in the frequency domain to facilitate assessment of impacts to effective beamwidth.

2.1 *Existing Cosine Windows*

Low elevation angles on the WSR-88D currently use the von Hann window in non-clutter regions. This window is defined with coefficients of $\alpha = 0.50$ and $\beta = 0.50$. Equivalent values of α and β give a shape of tapering with endpoints reaching the minimum amplitude value of 0.0. Torres and Curtis (2006, 2007) specifically selected the von Hann window in their study because it produces an effective beamwidth very close to the transmitted beamwidth, which was emphasized for small-scale feature detection in Base Data moments by others such as Brown et al. (2002) and Warde et al. (2005). Small-scale feature detection has not been emphasized for Dual-Polarization variables as strongly as Base Moments, so other windows can be considered.

A window similar in shape and feature to the von Hann is the Hamming window. Hamming coefficients are generally approximated to $\alpha = 0.54$ and $\beta = 0.46$. Figure 1 reveals the similarities of the von Hann and Hamming window in the time domain and frequency domain with regard to time-domain endpoints and frequency-domain main-lobe width. The Hamming window has endpoint amplitudes close to 0.08 instead of reaching the minimum value of 0.0. Main-lobe width in the frequency domain shows a Normalized Frequency of 0.26 for the Hamming and 0.27 for the von Hann. One notable difference is the first side-lobe magnitude in the frequency domain falling to -45 dB with the Hamming compared to -32 dB with the von Hann. Because this study is focused on non-clutter regions, the first side-lobe magnitude is a less critical factor than the main lobe width. Main lobe width is very similar for the von Hann and Hamming. Due to the extreme similarities of time-domain endpoints and frequency-domain main-lobe width, the Hamming window will not be considered for the remainder of the study.

Another commonly used and available window is the Rectangular window. Time-domain endpoints are maxed out at an Amplitude of 1.0; endpoints are as far away from the von Hann as possible (Figure 2). The corresponding frequency-domain main-lobe width is narrow Normalized Frequency of 0.13. These characteristics can lead to a wide effective beamwidth

which may not be preferred depending on the target type and phenomena of interest (Torres and Curtis, 2006).

Excluding cosine windows used for clutter regions, these three windows are the main named cosine windows used in the signal processing community. No named windows with coefficients between the Hamming and Rectangular have been explored with radar data. Because of the considerations for effective beamwidth on a rotating window, a new cosine window between the extreme ends of von Hann and Rectangular is explored.

2.2 *New Cosine Window (Meza)*

A window exactly halfway between the von Hann and Rectangular would have endpoints of 0.50 Amplitude in the time domain. To meet requirements that coefficients must be between 0.0 and 1.0 that both sum up to 1.0, a definition of $\alpha = 0.75$ and $\beta = 0.25$ is used. We refer to this set of coefficients as the Meza window because it falls in the middle between the von Hann and Rectangular in time-domain tapering (Figure 3).

An interesting difference occurs in the time-domain after transforming the Meza window (Figure 3). The main-lobe width is closer to the Rectangular with a Normalized Frequency of 0.16 instead of falling closer to halfway between the Rectangular and von Hann. A hypothesis arises that the Meza would thus have a lower impact on effective beamwidth than the Rectangular while maintaining higher statistical accuracy than the von Hann.

3. QUANTITATIVE COMPARISONS

3.1 *Estimator Bias and Standard Deviation*

Fewer samples, often associated with faster azimuthal rotation rates, present more challenges for accurately estimating moments and variables. We use settings from a fast rotation scanning strategy known as Volume Coverage Pattern (VCP) 12 to assess impacts in the most difficult retrieval mode; specifics can be found in the WSR-88D Interface Control Document for the RDA to RPG (WSR-88D ROC 2018b). Slower rates with more samples will have fewer impacts to bias and variance of estimators. In particular, we used the following parameters:

- M = 15 samples
- v_a = 8.05 m s^{-1}
- σ_v = 2.0 m s^{-1}

This corresponds to the minimum number of samples allowed for operational scanning strategies on the WSR-88D. Using a minimum number of samples puts the focus on situations that would have the most impact to the estimator based on the signal-processing window selection.

Simulated weather signals similar to the method in Zrnić (1975) and Torres (2001) were used to assess the bias and standard deviation of Dual-Polarimetric estimators. Bias and standard deviations (*SD*) for each are:

2

$$Bias\left(\widehat{X}\right) = \langle\widehat{X}\rangle - X \qquad (3.a)$$

$$SD\left(\widehat{X}\right) = \sqrt{\langle\left(\widehat{X} - \langle\widehat{X}\rangle\right)^2\rangle} \qquad (3.b)$$

where $\langle\ \rangle$ denotes the ensemble average, $\widehat{X}$ represents the estimator (ZDR, RHO, or PHI), and X is the true value of the estimated quantity. We used the following reference parameters for the simulations:

- ZDR_{Ref} = 1.0 dB
- RHO_{Ref} = 0.99
- PHI_{Ref} = 0.0 degrees[1].

Simulated signals were generated for five iterations of 100,000 samples for a total of 500,000 estimates per variable.

Figure 4 displays the resulting Bias estimates of ZDR, RHO, and PHI for the Rectangular, von Hann, and Meza windows. Each metric shows a similar story: the von Hann has noticeably more bias in each variable, the Meza has much less than von Hann, and the Rectangular has the least. The Meza window appears to have only a slight increase in bias compared to Rectangular, similar to the main-lobe width in the frequency domain plot. Figure 5 shows a similar pattern in the standard deviations of each DP variable. The Meza and Rectangular have reduced variance compared to the von Hann, and the Meza and Rectangular are quite close to each other visually in trend.

A percentage of change can be used to compare the amount of change between the windows. Because the existing operational window is von Hann, the Rectangular and Meza window will be compared to the von Hann. Mean percentage of change is calculated as:

$$Mean\ Percentage\ of\ Change = \left|\frac{Y-K}{K} \times 100\right| \qquad (4)$$

where Y represents the Bias(X) or SD(X) with X as the estimator of ZDR, PHI, or RHO for either the Rectangular or Meza window, K is the Bias or SD of a parameter using the von Hann window. The difference is taken at each SNR value; the mean of the differences results in a percentage of change relative to each type of window.

Results in Table 1 reveal that using a Rectangular window compared to a von Hann can have a reduction in estimator bias of 46-56%, and the Meza window has 35-46% reduction. The difference between the Rectangular and Meza is ~10% for each variable. Standard deviation is reduced up to 30-40% if using the Rectangular window while Meza window usage reduced the standard deviation down to 25-40% compared to the von Hann window. It is hypothesized that visual variability in non-derived data products would be reduced with the Meza and Rectangular windows compared to the existing von Hann. Our hypothesis is

---

[1] It should be noted that operational WSR-88D data use a non-zero starting reference PHI value known as the Initial System Differential Phase. That value is not important for the signal simulations, thus 0.0 is acceptable as a reference PHI for corresponding to the beginning of simulated weather signals.

explored later in the Qualitative Comparisons section, but this is not the only factor of influence on the visual aspect of the data. Effective beamwidth also plays an important role in visual interpretation of raw data and potentially in derived products.

TABLE 1. Mean Percentage of Change in bias and standard deviation for each DP Estimator compared to using the von Hann window. Negative values represent a decrease in bias and standard deviation, thus corresponding to an improvement.

		Meza	Rectangular
Bias	ZDR	-35%	-46%
	RHO	-46%	-56%
	PHI	-36%	-51%
Standard Deviation	ZDR	-25%	-32%
	RHO	-39%	-45%
	PHI	-26%	-31%

3.2 *Effective Beamwidth Comparison*

Equation 2 shows that the number of samples, *M*, is a factor in the effective beamwidth based on the azimuthal rotation rate and the window. A rotation rate of 21.15° s^{-1} is used to match the Nyquist velocity (v_a) of 8.05 m s^{-1} on the WSR-88D and is coupled with the theoretical radiation pattern given in Doviak and Zrnić (1998) to simulate impacts to the effective beamwidth based on window selection. Figure 6 compares the three signal processing windows to the natural beamwidth transmitted when the antenna is not rotating. Numerically, the difference in effective beamwidths between the von Hann and Rectangular is -0.36%, signifying the degradation of azimuthal resolution due to the increase in effective beamwidth if using the Rectangular window. The difference between the von Hann and Meza is -0.17%, which is approximately half of the difference if using a Rectangular window.

Increase in the effective beamwidth is also apparent in the estimated effective antenna patterns shown in Figure 6. Broadening the effective beamwidth can lead to a visual appearance of smearing data in azimuth, which may be less desired for target and/or phenomena detection in dual-polarization variables.

4. QUALITATIVE COMPARISONS

4.1 *Non-Derived Products*

We previously introduced ideas of how the bias, standard deviation, and effective beamwidth could appear visually in the data. Specifically:

1) Reduced standard deviation should translate to less variation in the raw products assessed visually.
2) Increasing the effective beamwidth can translate into products appearing to have smeared data in the azimuthal direction.

Six data cases, listed in Table 2, were visually assessed by a team of radar experts for differences with the different signal processing windows. These cases use raw In-phase and Quadrature data collected from

the site. Such data files are large and difficult to store/collect, hence the relatively low number of test cases here. The WSR-88D software packages low-elevation angle data into radar range gate sizes of 0.25 km X 0.5°. The radar range gate size will not change based on the signal processing window, but the estimation of signal within each bin can as shown by the bias, standard deviation, and effective beamwidth metrics may impact the visual grouping of data. Examples from three of the six cases are discussed.

TABLE 2. List of cases analyzed using their In-Phase and Quadrature data.

Radar	Date	Time (UTC)	VCP	Description
DAN1	20130531	2301-2354	212	Heavy precipitation tornadic supercells
KMHX	20110624	1301-1459	21	Hurricane rain bands far offshore; Anomalous Propagation near shore.
KOUN	20110109	1815-1837	21	Mixed winter precipitation
KOUN	20110524	1922-2353	12	Tornado outbreak
KPUX	20130721	0500-0737	212	Convection over mountains
KVNX	20110424	0936-1118	11	Stratiform rain (north) and convection (south)

A tornadic supercell case from 31 May 2013 (Figure 7) shows a well-defined hook echo associated with a tornadic vortex, areas of hail, and heavy precipitation from the entire storm. The tornadic signature is ~56 km (~30 nmi) northwest of the radar at 297° in azimuth. The inflow notch associated with the tornado has clear signatures in Z, W, ZDR, and RHO at this time. Comparing the visual aspects of these features with decreasing tapering reveals how decreased standard deviation of estimators corresponds to an image with less visual variance giving off a smoother appearance. Dual-polarimetric signatures with the Meza window isolated the details of the inflow notch and tornadic vortex region compared to the von Hann. Increasing the effective beamwidth with the Rectangular results in features appearing more azimuthally smeared. All of the important storm features are visible with any of the three windows, but less-tapered windows produce estimates with less fluctuation which may result in the improved visual separation of individual features that could facilitate faster visual analysis of the meteorological event in real-time.

Figure 8 shows a different tornadic supercell event from 24 May 2011 where a leading area of rain developed in front of the established tornado, causing the signature to become rain-wrapped. The tornadic signature is ~72 km (~39 nmi) northwest of the radar at 292° azimuth. Signatures of the isolated hail regions and inflow regions are more difficult to distinguish with the von Hann window. Moving to the Meza window, the inflow region of the tornado and the updraft region of the storm developing southeast of the tornado become isolated features in ZDR. Immediately north and northwest of the tornado, small regions of

hail appear as separate groups of lower RHO values with the Meza window compared to the visual variance of the von Hann window. The impact is repeated in the Rectangular, though the increased effective beamwidth gives less resolution to the small isolated hail regions. Low RHO value regions northwest of these isolated groups and southeast of the tornado are caused by attenuation related to the hail from the main supercell and the convective thunderstorm southeast of the tornado being ingested into the stronger mesocyclone. Attenuation effects in PHI are relatively large scale with little difference between window selections, yet a small circular signature is apparent in PHI when using the von Hann or Meza window. This small feature loses its circular pattern in PHI when using a Rectangular window. Signatures in ZDR and RHO with a Rectangular window are otherwise similar to the Meza with the added visual effect of azimuthal smearing.

A difficult environment to interpret can come from mixed-phase winter precipitation events (Figure 9). An example from 09 January 2011 highlights one of the largest benefits of polarimetric data – particle type discernment. Z, V, and W values all appear similar across the region, while the DP variables show separate sections of other particle types. At the radar approximately ~74 km (40 nmi) south of this region, temperatures were freezing at the surface with a warm layer aloft contributing to melting snow and ice crystals. Patches of melting particles become well-defined regions in ZDR and RHO with reduced tapering of the signal processing window. Interestingly, the PHI begins as a relatively intense notable region of melting particles with the von Hann and Meza that appears reduced in intensity when using a Rectangular window. The authors admit this could partially be related to color scale selection and not solely an impact of the increased effective beamwidth.

Less-tapered windows have a visual impact on high-resolution non-derived products. Overall visual variance is reduced which separates specific meteorological features more clearly. A side effect of reducing the tapering completely (e.g., by using a Rectangular window) is the appearance of smearing in azimuth. Such changes in high-resolution products could impact other products derived from the high-resolution data.

4.2 *Derived Products*

The highest resolution of raw data from the WSR-88D comes packaged in radar range gates of 0.25 km X 0.5° azimuth as shown in Figures 7-9. The initial step for calculating derived products involved repackaging these high-resolution range gates into 0.25 km X 1.0°. Algorithms may further repackage data into 1.0 km X 1.0°. These larger groups are often used with a 3 X 3 neighborhood weighting schemes for statistical metric calculations. Elevation resolution is always 1.0° for single-elevation angle data processing regardless of the range and azimuth packaging (OFCM 2017).

Figure 10 displays an example high-resolution data repackaging options used for derived product algorithms. Light blue boxes represent 0.25 km X 1.0°

4

grouping equating to two high-resolution radar range gates. Black boxes represent 1.0 km X 1.0° grouping equating to twelve high-resolution range gates. As the grouping expands, the differences between range gates apparent in the high-resolution data would be averaged out (not shown with the Figure). Thus, it is unlikely that the effects of less-tapered windows will be noticeable in derived products.

One derived product to test this claim is the Digital Hydrometeor Classification (DHC) product. The DHC uses 0.25 km X 1.0° groupings and creates a product for each separate elevation angle. Output DHC from the 09 January 2011 case in Figure 11 matches the region and time shown in Figure 9. As expected with the melting snow/ice crystal signature, a large area of this region has been classified as Big Drops with some Wet Snow scattered throughout. Dry snow covers much of the area outside of the Big Drops with some areas of Ice Crystals throughout. Main features have little to no difference between the signal-processing windows, yet the northeast region of Big Drops shows a reduction in the number of radar bins marked as Ground Clutter when using a less-tapered window. This is a positive improvement as we previously mentioned how polarimetric variables are more sensitive to noise impacts from ground clutter.

Tornadic supercells also pose interesting challenges in Hydrometeor Classification. Figure 12 shows the DHC products from the 24 May 2011 time and region in Figure 8. Isolated bins of Hail seen with the von Hann window are removed as the variance of the estimators improves with decreased tapering of the signal-processing window. Bins marked as Hail in the Meza and Rectangular window products match with the descriptions discussed earlier with the non-derived, high-resolution products. Otherwise, except for a few isolated bins scattered throughout, the overall detections of the DHC remain the same regardless of windowing selection. An interesting isolated bin to note is one near the inflow region near the tornadic signature. Information from the Meza window shows the inflow notch more detailed than the Rectangular window. This could be from random calculation chance rounding in the computer or related to the increase in effective beamwidth as data from nearby returns smear into the estimation range for this bin.

Finally, a derived product often requested from radar data is precipitation estimation. The Digital Storm Total Accumulation Product (DSA) uses the Quantitative Precipitation Estimation (QPE) algorithm to determine the total amount of rainfall since the beginning of a storm event. (OFCM 2017). The QPE algorithm uses data from multiple elevation angles, so decreased variance at only the lower elevation angles may have little to no difference in rainfall totals. Figure 13 shows the example associated with the heavy precipitation supercell from 31 May 2013 shown in Figure 7. Overall structures and amounts are similar between the three signal processing windows. An interesting region of differences does appear in the attenuation regions in the far left portion of the image. Less-tapered windows show more continuous regions with slightly higher precipitation totals in areas of attenuation. It is likely this is a direct result of decreasing bias and standard deviation across the field of estimators.

5. SUMMARY AND DISCUSSION

Polarimetric radar variable estimators are more sensitive to impacts of noise than Base moments. This can lead to increased variance of the polarimetric variable estimates whereby the selection of signal-processing window can either mitigate or exacerbate this effect. WSR-88D radars use the von Hann window for Base Moments to achieve a specific effective beamwidth, yet this leads to noticeably increased visual variance in non-derived polarimetric products. Two less-tapered windows are explored as a way to decrease the estimator variability while considering the goals of maintaining a small effective beamwidth.

A Rectangular window significantly reduces the bias and standard deviation of polarimetric estimators up to ~40-50%. On the reverse, the azimuthal resolution is degraded by 36% due to the increase in effective beamwidth. In raw visual comparisons of non-derived products, the Rectangular window has reduced visual variance to match the reduction in standard deviation while adding the appearance of azimuthal smearing of signals. The smeared appearance is less desirable for non-derived products because users often compare polarimetric signatures to Base Moments and are expected to match in location and extent.

Because the von Hann window has some of the most tapering available in regions without clutter and the Rectangular has the least, a cosine window with tapering characteristics halfway between these extremes was defined for use with polarimetric variables. The authors have dubbed this cosine coefficient set the Meza window. Bias and standard deviation calculations for polarimetric estimators show reductions of ~30-40%, only ~10% less than the Rectangular window. The azimuthal resolution is degraded by 17% as a tradeoff for the improved estimations, approximately half of the degradation seen with the Rectangular window. Non-derived products show the benefits of decreasing bias and standard deviation while reducing impacts to effective beamwidth. Important meteorological signatures separate into well-defined visual groups without giving an appearance of azimuthal smearing. Less azimuthal smearing can facilitate comparisons of features with Base Moment data and provide confidence in distinguishing the extent of isolated features such as small hail cores, inflow notches, phase change regions, etc.

Visually, the improvements of using a less-tapered window are most noticeable in the high-resolution raw products available due to the way high-resolution range gates are grouped together into lower resolutions for derived product calculation. The winter weather example did show a benefit in Hydrometeor Classification in that the total number of bins marked as Ground Clutter were reduced with a less-tapered window. One of the tornadic cases showed an improved definition of an inflow notch when using the Meza window compared to the von Hann or Rectangular. Precipitation accumulation showed improvement with a less-tapered window, but little difference between the Meza window and the Rectangular window. Results from the Rectangular have some

5

smeared regions that give the appearance of continuity due to the increased effective beamwidth, but the differences compared to the Meza window are small.

The Meza window stands out as a good balance between decreasing bias and standard deviation with less impact to effective beamwidth. It is recommended that a less-tapered window such as the Meza window be used for polarimetric variables in regions without clutter to improve the visual appearance of non-derived products used for interpretation of meteorological features. Derived products using the data with less bias and standard deviation without azimuthal smearing show some improvement in feature detection as well, though the lower resolution groupings used by algorithms can make the differences appear negligible. Data were not impacted negatively when using the Meza window compared to the von Hann window, so the window is acceptable for operational use.

6. ACKNOWLEDGEMENTS

7. REFERENCES

Brown, R.A., V.T. Wood, and D. Sirmans, 2002: Improved Tornado Detection Using Simulated and Actual WSR-88D Data with Enhanced Resolution. J. Atmos. Oceanic Technol., 19, 1759–1771, https://doi.org/10.1175/1520-0426(2002)019<1759:ITDUSA>2.0.CO;2.

Crum, T.D., R.L. Alberty, and D.W. Burgess, 1993: Recording, Archiving, and Using WSR-88D Data. Bull. Amer. Meteor. Soc., 74, 645–654, https://doi.org/10.1175/1520-0477(1993)074<0645:RAAUWD>2.0.CO;2.

Doviak, R. J., and D.S. Zrnić, 1998: Polarimetric upgrades to Improve Rainfall Measurements. National Severe Storms Laboratory Report, pp. 110. [Available online at https://www.nssl.noaa.gov/publications/wsr88d_reports/2pol_upgrades.pdf.]

Doviak, R. J., V. Bringi, A. Ryzhkov, A. Zahrai, and D. Zrnić, 2000: Considerations for Polarimetric Upgrades to Operational WSR-88D Radars. J. Atmos. Oceanic Technol., 17, 257–278, https://dx.doi.org/10.1175/1520-0426(2000)017<0257:CFPUTO>2.0.CO;2.

Doviak, R. J. and D.S. Zrnić, 2006: Doppler radar and weather observations. 2nd ed. Dover Publications, 562 pp.

Harris, F. J., 1978: On the use of windows for harmonic analysis with the discrete Fourier transform. Proc. IEEE, 66, 51-83, https://doi.org/10.1109/PROC.1978.10837.

Melnikov, V., and D. S. Zrnić, 2004: Simultaneous transmission mode for the polarimetric WSR-88D: Statistical biases and standard deviations of polarimetric variables. NOAA/NSSL Rep., 84 pp. [Available online at http://cimms.ou.edu/~schuur/jpole/SHV_statistics.pdf].

Melnikov, V.M. and D.S. Zrnić, 2007: Autocorrelation and Cross-Correlation Estimators of Polarimetric Variables. J. Atmos. Oceanic Technol., 24, 1337–1350, https://doi.org/10.1175/JTECH2054.1.

OFCM, 2017: WSR-88D Meteorological Observations. Part C: WSR-88D Products and Algorithms. Federal Meteorological Handbook, No. 11, OFCM, Dep. Of Commerce, 394 pp. [Available online at https://www.ofcm.gov/publications/fmh/FMH11/fmh11partC.pdf.]

Saxion, D. S., R. D. Rhoton, R. L. Ice, G. T. McGehee, D. A. Warde, O. E. Boydstun, W. D. Zittel, S. Torres, G. Meymaris, 2007: New Science for the WSR-88D: Implementing a Major Mode On the SIGMET RVP8, 23rd International Conference on Interactive Information Processing Systems for Meteorology, Oceanography, and Hydrology. [Available online at https://ams.confex.com/ams/pdfpapers/119062.pdf.]

Siggia, A., and J. R. Passarelli, 2004: Gaussian model adaptive processing (GMAP) for improved ground clutter cancellation and moment calculation. Proc. Third European Conf. on Radar in Meteorology and Hydrology, Visby, Gotland, Sweden, ERAD, 67–73. [Available online at https://www.copernicus.org/erad/2004/online/ERAD04_P_67.pdf.]

Torres, S. M., 2001: Estimation of Doppler and polarimetric variables for weather radars. Ph.D. dissertation, University of Oklahoma, 158 pp. [Available online at https://shareok.org/handle/11244/361.]

Torres, S., and C. Curtis, 2006: Design considerations for improved tornado detection using super-resolution data on the NEXRAD network. Proc. Fourth European Conf. on Radar in Meteorology and Hydrology, Barcelona, Spain, Servei Meteorològic de Catalunya. [Available online at http://cimms.ou.edu/~torres/Documents/ERAD%202006.pdf.]

Torres, S., and C. Curtis, 2007: Initial implementation of super-resolution data on the NEXRAD network. Preprints, 23rd Int. Conf. on Interactive Information and Processing Systems for Meteorol-

ogy, Oceanography, and Hydrology, San Antonio, TX, Amer. Meteor. Soc., 5B.10. [Available online at http://ams.confex.com/ams/pdfpapers/116240.pdf.]

Torres, S.M. and D.A. Warde, 2014: Ground Clutter Mitigation for Weather Radars Using the Autocorrelation Spectral Density. J. Atmos. Oceanic Technol., 31, 2049–2066, https://doi.org/10.1175/JTECH-D-13-00117.1.

Warde, D. A., R. L. Ice, R. D. Rhoton, D. S. Saxion, and D. Sirmans, 2005: Radar Operations Center (ROC) Engineering Evaluation of Proposed Super Resolution Techniques. 21st International Conference on Interactive Information Processing Systems for Meteorology, Oceanography, and Hydrology. [Available online at https://ams.confex.com/ams/pdfpapers/85894.pdf.]

Warde, D.A. and S.M. Torres, 2017: Staggered-PRT Sequences for Doppler Weather Radars. Part II: Ground Clutter Mitigation on the NEXRAD Network Using the CLEAN-AP Filter. J. Atmos. Oceanic Technol., 34, 703–716, https://doi.org/10.1175/JTECH-D-16-0072.1

WSR-88D ROC, 2008: Interface Control Document for the Product Specification: RPG Build 10.0, 2620003L, WSR-88D Radar Operations Center. [Available online at https://www.roc.noaa.gov/wsr88d/PublicDocs/ICDs/2620003L.pdf.]

WSR-88D ROC, 2010: Interface Control Document for the Product Specification: RPG Build 12.0, 2620003P, WSR-88D Radar Operations Center. [Available online at https://www.roc.noaa.gov/wsr88d/PublicDocs/ICDs/2620003P.pdf.]

WSR-88D ROC, 2013: NEXRAD/WSR-88D History. Radar Operations Center. Accessed 18 Dec 2017.[Available online at https://www.roc.noaa.gov/WSR88D/PublicDocs/NEXRAD.pdf.]

WSR-88D ROC, 2018a: WSR-88D system specification revision K. NWS Radar Operations Center Rep. ROC/2810000K/0WY55, 162 pp.

WSR-88D ROC, 2018b: Interface Control Document for the RDA/RPG: RDA Build 18.0, 2620002R, WSR-88D Radar Operations Center. [Available online at https://www.roc.noaa.gov/wsr88d/PublicDocs/ICDs/RDA_RPG_2620002R.pdf.]

Zrnić, D. S., 1975: Simulation of weatherlike Doppler spectra and signals. J. Appl. Meteor., 14, 619–620, doi:https://doi.org/10.1175/1520-0450(1975)014<0619:SOWDSA>2.0.CO;2.

Zrnić D. S., and R. J. Doviak, 1976: Effective antenna pattern of scanning radars. IEEE Trans. Aerosp. Electron. Syst., AES-12, 551-555, https://doi.org/10.1109/TAES.1976.308254.
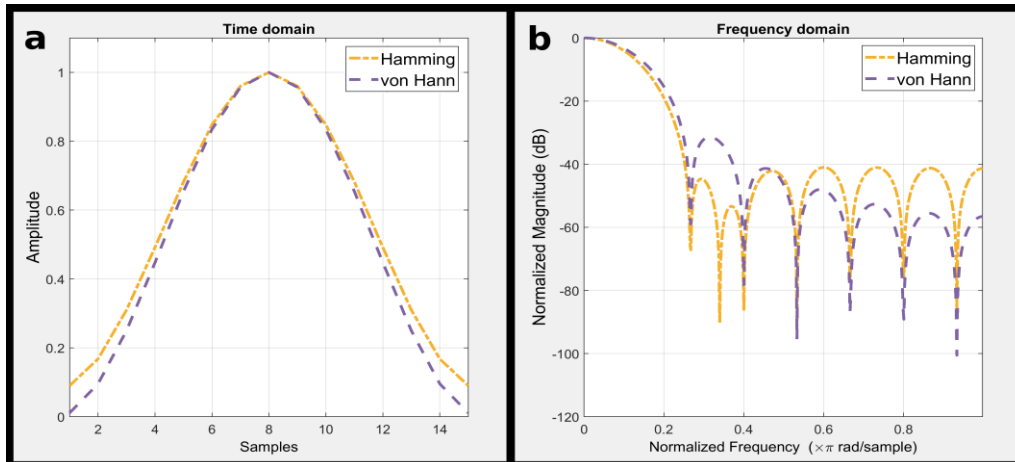
8.   FIGURES

FIGURE 1. Window shapes and characteristics in the Time and Frequency domain for the Hamming (yellow dot-dash) and von Hann (purple dash) windows when using $M = 15$ samples. The Frequency Domain information is obtained by taking the Fast Fourier Transform of the Time Domain.
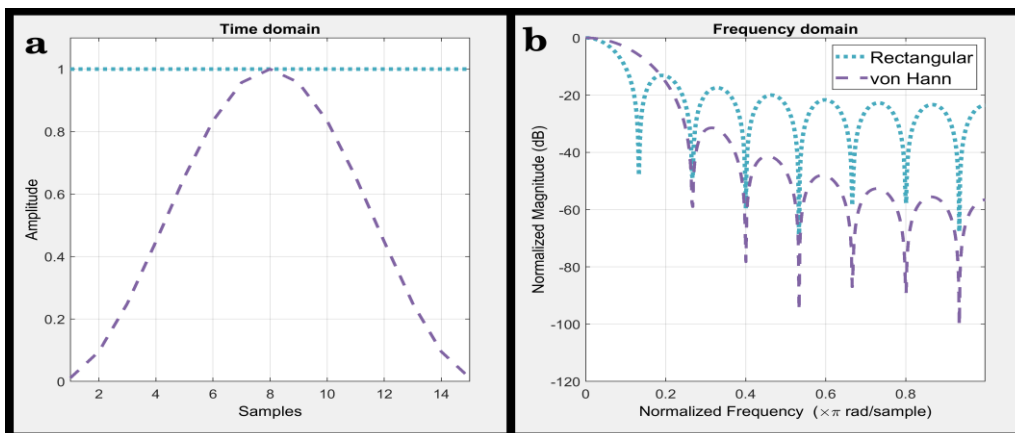
FIGURE 2. Window shapes and characteristics for the Rectangular (blue dot) and von Hann (purple dash) windows.
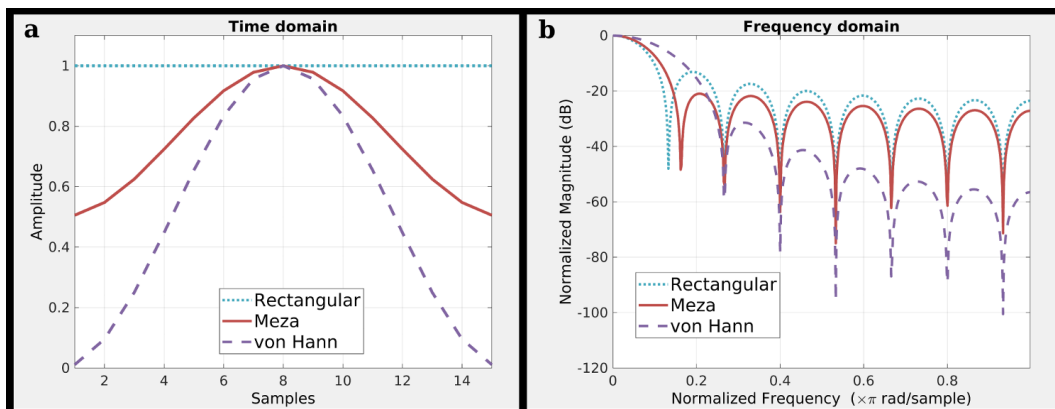
FIGURE 3. Window shapes and characteristics for the Rectangular (blue dot), Meza (red solid), and von Hann (purple dash) windows. These three windows are the ones tested throughout the study.

8
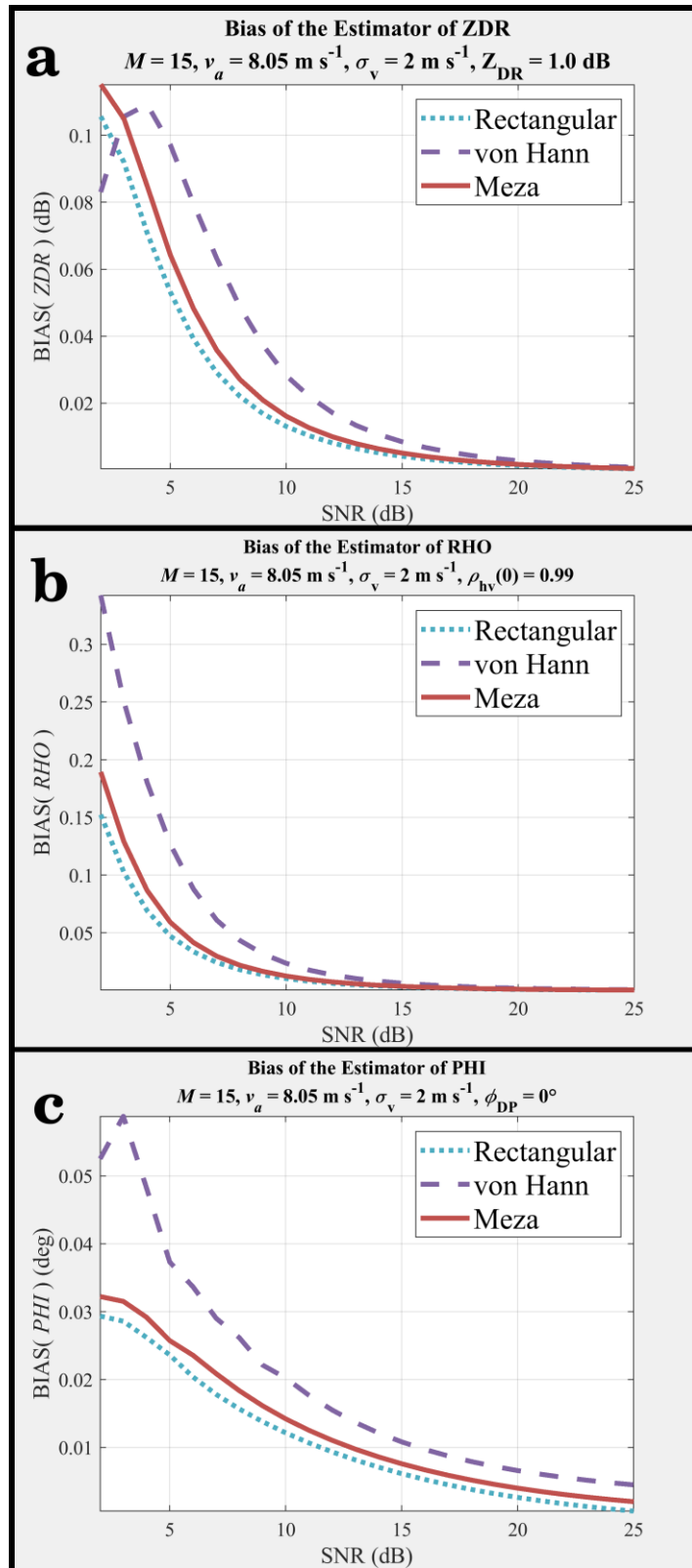
FIGURE 4. Bias of the estimators of ZDR (a), RHO (B), and PHI (C) in relation to increasing Signal-to-Noise Ratio based on simulations of Time Series weather signals using WSR-88D VCP 12 operating samples and Nyquist velocity according to the WSR-88D Interface Control Document (WSR-88D ROC 2018b).

a Standard Deviation of the Estimator of ZDR

$M = 15$, $v_a = 8.05$ m s^{-1}, $\sigma_v = 2$ m s^{-1}, $Z_{DR} = 1.0$ dB

b Standard Deviation of the Estimator of RHO

$M = 15$, $v_a = 8.05$ m s^{-1}, $\sigma_v = 2$ m s^{-1}, $\rho_{hv}(0) = 0.99$

c Standard Deviation of the Estimator of PHI

$M = 15$, $v_a = 8.05$ m s^{-1}, $\sigma_v = 2$ m s^{-1}, $\phi_{DP} = 0°$
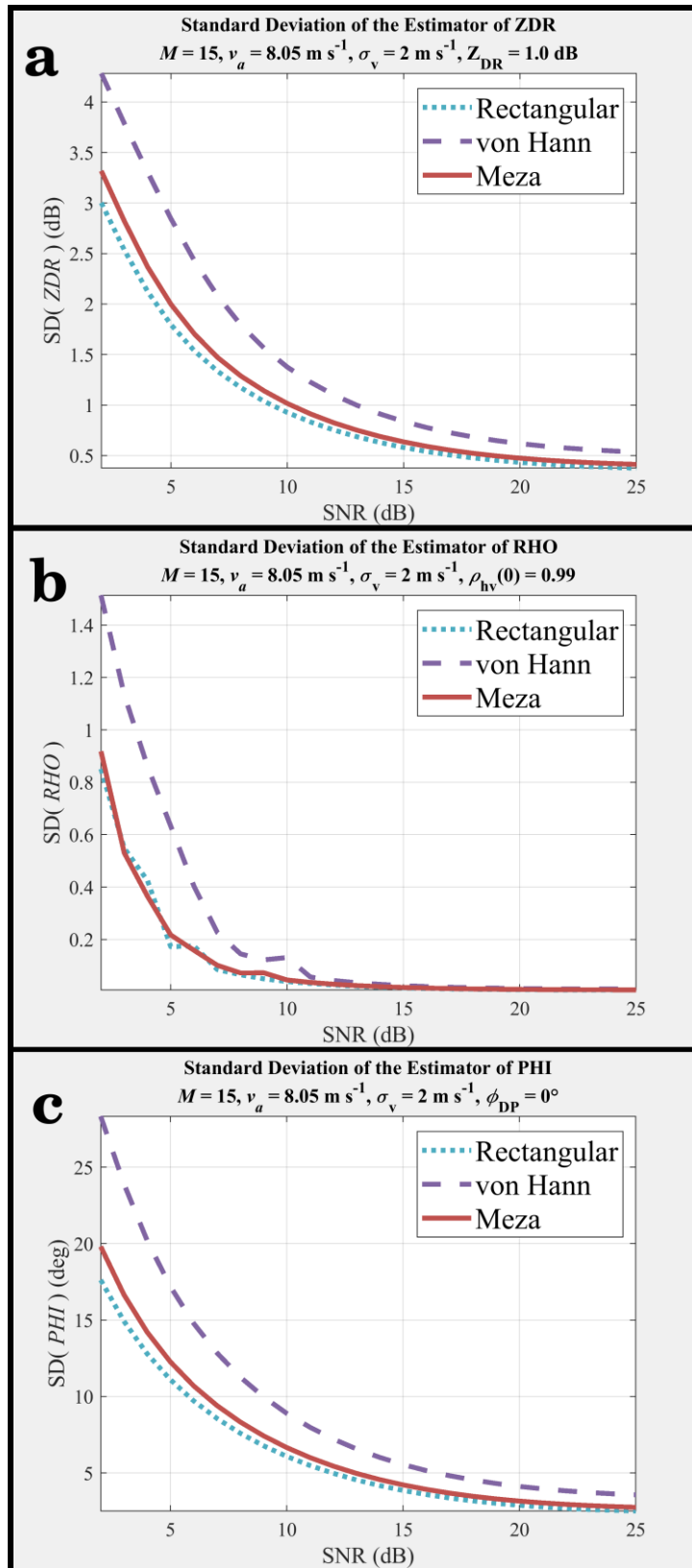
FIGURE 5. Same as Figure 4 but for the Standard Deviation of the Estimator in relation to increasing SNR.
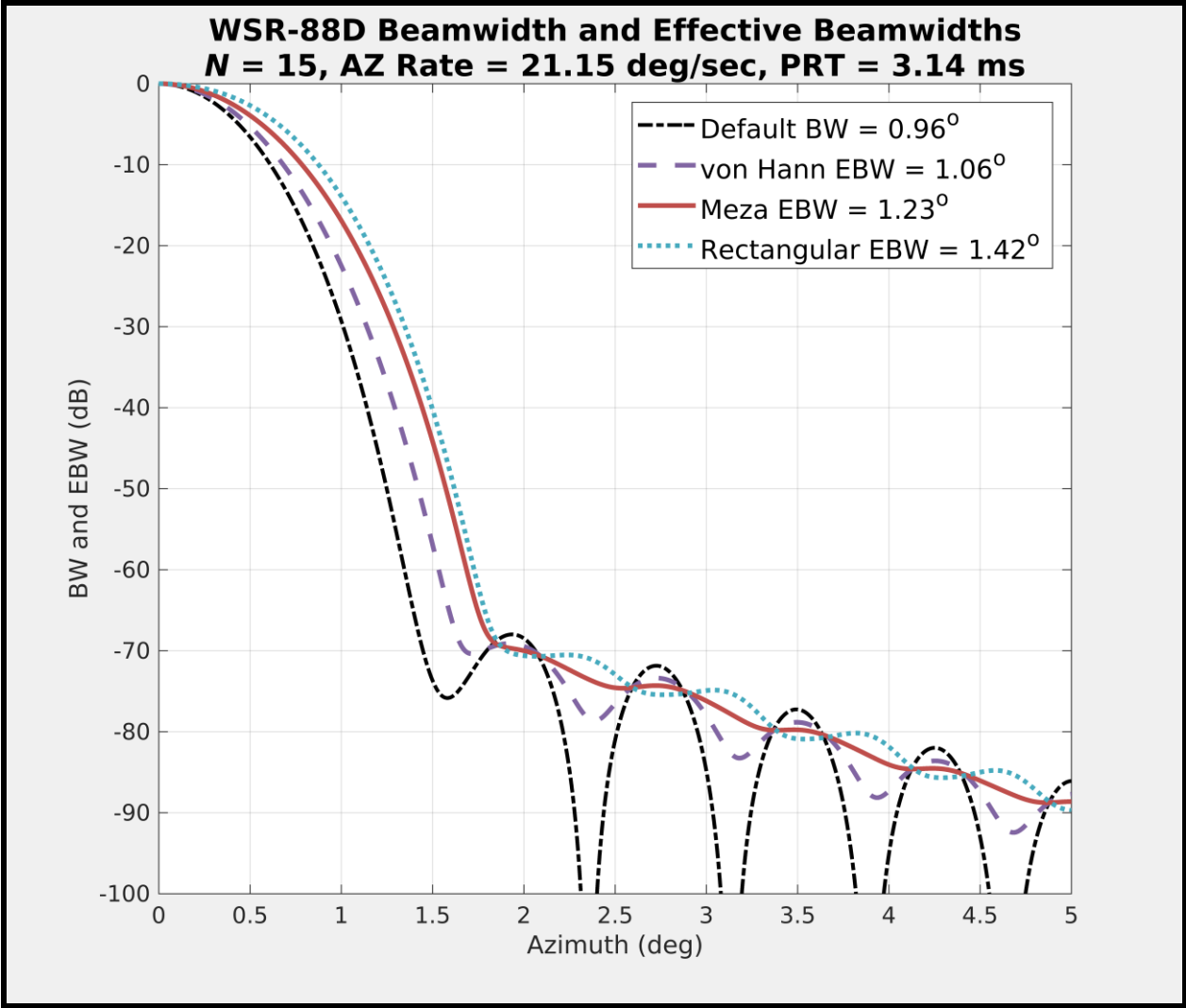
FIGURE 6. Natural transmitted beamwidth pattern of the WSR-88D (black dash) and associated effective beamwidths based on the signal processing window selection using VCP 12 operational parameters.
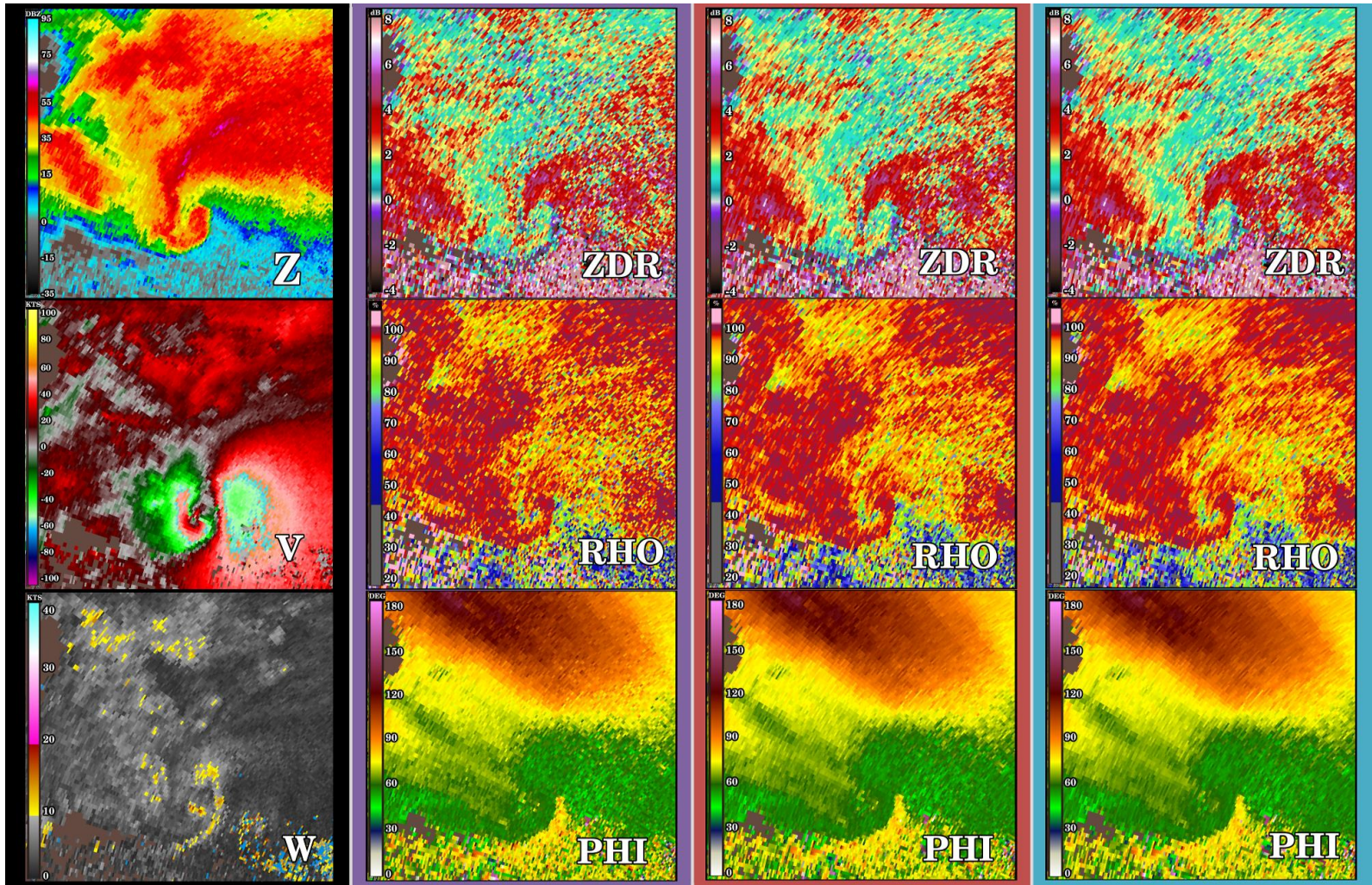
FIGURE 7. Visual example of non-derived data from the DAN1 20130531 Case for elevation 0.5° at 23:11 UTC. The radar is located southeast of view section which has zoomed onto the tornadic hook echo signature ~56 km away from the radar. The first column on the left shows the Base Moments; these are unaffected by the signal processing window changes in this study. The Second column shows Dual-Polarimetric results from the current operational standard von Hann window. Meza window results are shown in the third column, and rectangular window results are in the fourth column.
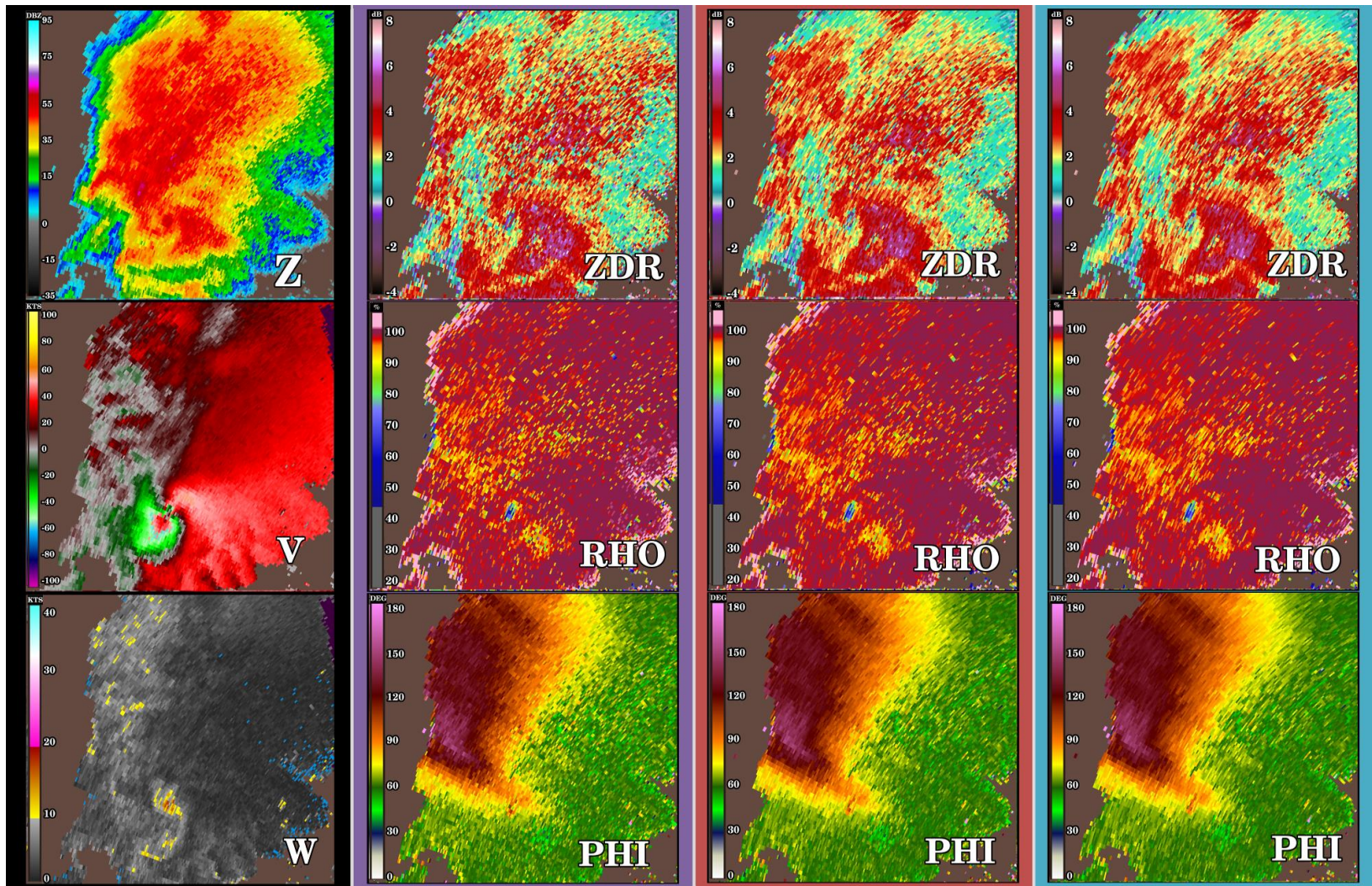
FIGURE 8. Similar to Figure 7 but for the KOUN 20110524 Case at elevation 0.5° at 21:01 UTC focusing on a tornadic supercell ~72 km away from the radar located to the southeast of the image.

FIGURE 9. Similar to Figure 7 and 8 but for the KOUN 20110109 case at 0.5° elevation at 18:30 UTC. The area of mixed phase precipitation in the image is located ~74 km north of the radar location.

14
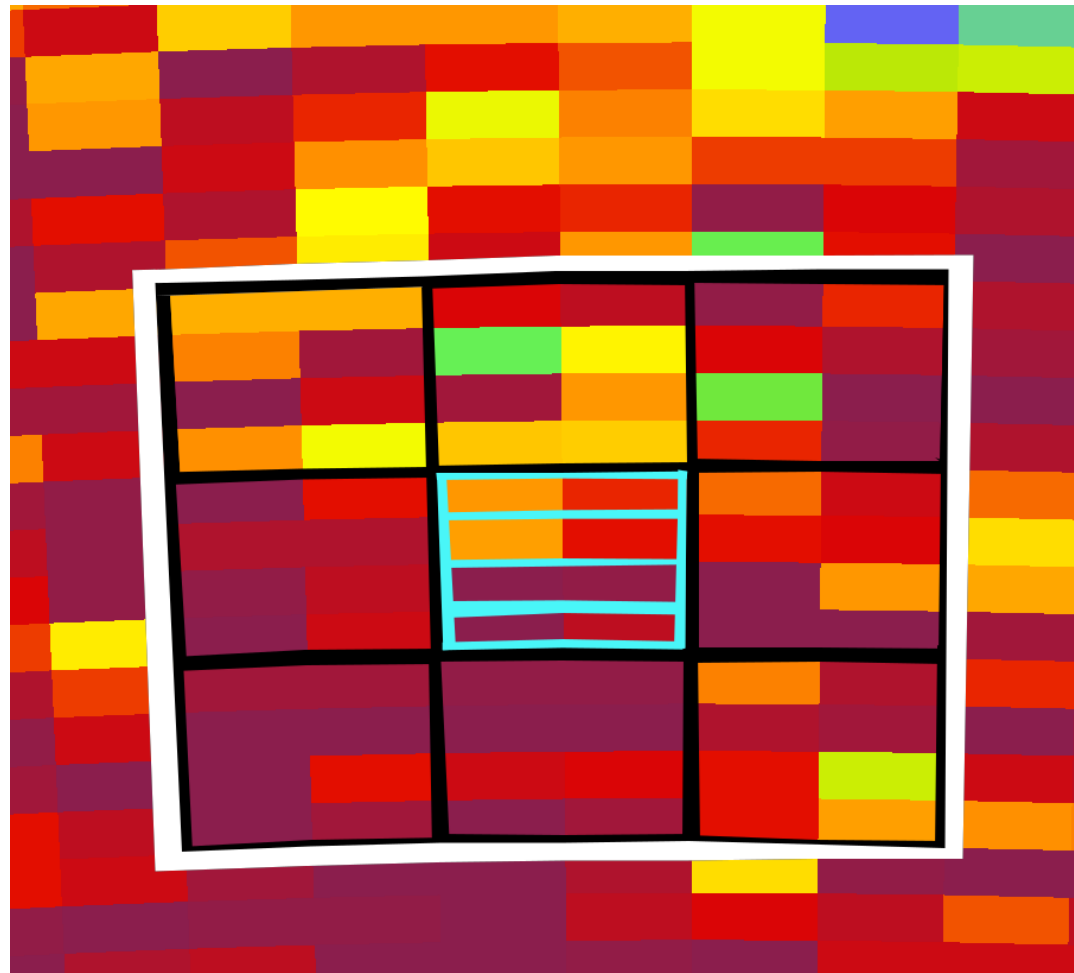
FIGURE 10. Graphic example of how high-resolution data from non-derived products can be grouped or used for statistics in derived products. The Light blue boxes represent the highest possible resolution available for derived products. Other products use sizes related to the Black boxes. Finally, groups of black boxes in a 3 X 3 neighborhood may be used with weighting schemes to calculate statistics for the Black Box in the center of the neighborhood. As the grouping grows, the high-resolution details are averaged out.
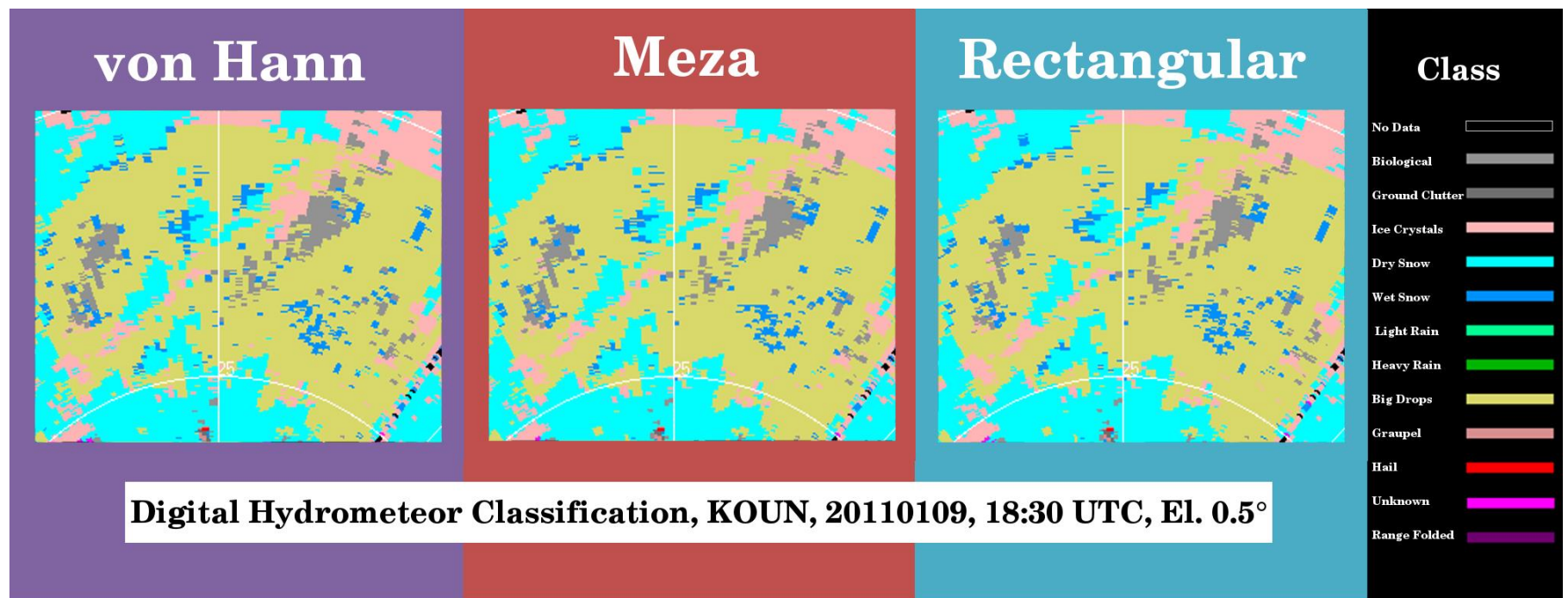
FIGURE 11. Digital Hydrometeor Classification derived product showing the same region as Figure 9 for the winter weather precipitation case.
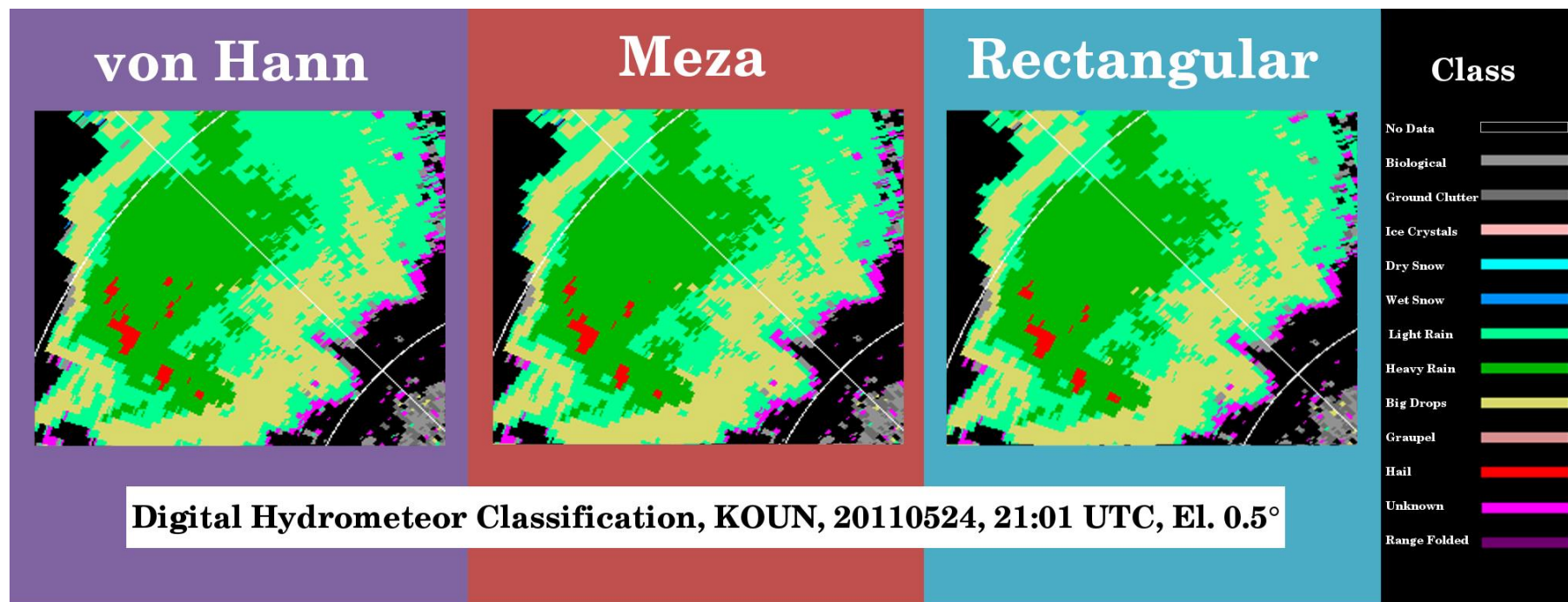
FIGURE 12. Digital Hydrometeor Classification for the same region shown in Figure 8.
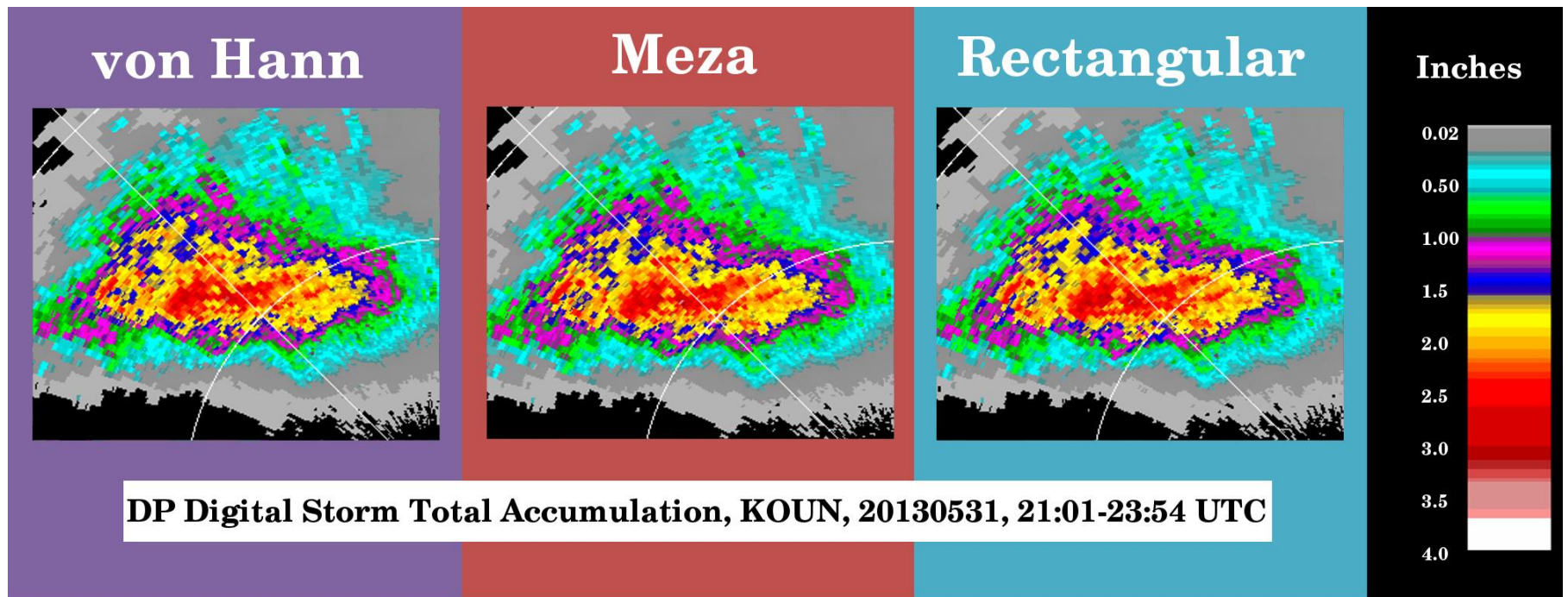
FIGURE 13. Dual-Polarimetric Storm Total Accumulation for the Heavy Precipitation Supercell case from DAN1 on 20130531.